IOPscience iopscience.iop.org

Home Search Collections Journals About Contact us My IOPscience

High-resolution photoinduced transient spectroscopy as a new tool for quality assessment of semi-insulating InP

This article has been downloaded from IOPscience. Please scroll down to see the full text article.

2004 J. Phys.: Condens. Matter 16 S225

(http://iopscience.iop.org/0953-8984/16/2/027)

View the table of contents for this issue, or go to the journal homepage for more

Download details:
IP Address: 129.252.86.83
The article was downloaded on 28/05/2010 at 07:44

Please note that terms and conditions apply.

J. Phys.: Condens. Matter **16** (2004) S225–S233 PII: S0953-8984(04)66911-6

High-resolution photoinduced transient spectroscopy as a new tool for quality assessment of semi-insulating InP

P Kaminski, R Kozlowski[1], S Strzelecka and M Piersa

Institute of Electronic Materials Technology, ulica Wolczynska 133, 01-919 Warszawa, Poland

E-mail: kozlow-r@itme.edu.pl

Received 31 July 2003
Published 22 December 2003
Online at stacks.iop.org/JPhysCM/16/S225 (DOI: 10.1088/0953-8984/16/2/027)

Abstract
High-resolution photoinduced transient spectroscopy has been applied to study grown-in defect centres in semi-insulating InP:Fe. The defect structure of crystals characterized by various values of Hall mobility has been compared. A number of defect centres with activation energies ranging from 10 to 640 meV were detected. They include shallow donor and acceptor impurities, native defects, shallow impurity–native defect complexes and iron-related defects. It was found that the Hall mobility is mainly affected by the shallow donor concentration which determines the ratio $[Fe^{2+}]/[Fe^{3+}]$. The electron lifetime is determined either by the iron concentration or the concentration of shallow impurities.

1. Introduction

Semi-insulating InP:Fe is a very important material in terms of applications in advanced microelectronics and optoelectronics. Most frequently, InP crystals are grown by a high-pressure liquid encapsulated Czochralski (LEC) method. The semi-insulating properties of InP crystals are usually obtained by doping with iron, forming a deep acceptor level compensating residual shallow donors resulting from contamination with silicon and sulfur atoms [1]. The typical concentration of iron is in the range of (1–5) $\times$ 10^{16} cm^{-3}. The electronic properties of point defects in semi-insulating InP are poorly understood. It has been established that the energy level related to phosphorus antisite $P_{In}^{0/+}$ is located above the bottom of the conduction band at $E_c + 0.12$ eV [2]. The second energy level related to the antisite $P_{In}^{+/2+}$ is located at $E_c - 0.23$ eV [2]. The activation energy for electron emission from the Fe^{2+} centre is 0.64 eV [3]. However, according to the results obtained by thermally stimulated current (TSC) and photoinduced transient spectroscopy (PITS), a number of observed defect centres have not

[1] Author to whom any correspondence should be addressed.

been identified. Moreover, it is not clear how the iron concentration and the growth conditions affect the material defect structure.

In this work, high-resolution photoinduced transient spectroscopy (HRPITS) is used for the quality assessment of SI InP:Fe. This technique is a greatly improved version of the classical photoinduced current transient spectroscopy first used by Hurtes *et al* [4] and Fairman *et al* [5] to investigate deep traps in SI GaAs. Using the HRPITS technique, the photocurrent decays in SI InP:Fe are measured in a wide range of temperatures (20–320 K) and analysed for a broad range of emission rate windows from $\sim 4 \times 10^2$ to 5×10^5 s^{-1}. The electronic properties of a number of defect centres in the crystals with different iron concentration and characterized by different values of Hall mobility are compared.

2. Experimental details

The samples for studies of defect centres were prepared from the (100) wafers originated from the SI InP:Fe ingots grown by LEC technique. The wafers' thickness was ~ 450 μm. The samples were characterized by measurements of resistivity and Hall mobility at 300 K as well as by the measurements of iron concentration and the temperature dependence of dark current (TDDC). The Fe concentration was determined by secondary ion mass spectroscopy (SIMS). The parameters of the samples are summarized in table 1.

Table 1. The parameters of the SI InP:Fe samples used for the investigation of defect centres.

Sample	Resistivity at 300 K (Ω cm)	Hall mobility at 300 K (cm^2 V^{-1} s^{-1})	[Fe] (cm^{-3})	E_{TDDC} (eV)
218it	2.0×10^7	1600	1.0×10^{16}	0.51
21aym	1.47×10^8	2392	4.0×10^{16}	0.59
24asd	1.43×10^8	2638	9.0×10^{15}	0.63

According to the data given in table 1, we have chosen the samples with different Hall mobility and various iron concentrations. It should be noted that the Hall mobility is correlated with the activation energy determined from the TDDC measurements. This energy can be considered as the Fermi level position extrapolated to 0 K, and it indicates the grade of the material contamination with shallow donors. In other words, the higher the value of E_{TDDC} the lower the concentrations of shallow donors.

For HRPITS measurements, arrays of Au ohmic contact pairs were deposited on the polished surface of the wafers. The gap between two electrodes was 0.7 mm. The wafers were cut into chips of 4×9 mm^2 in area, which were mounted in the sample holder of a cryostat. The experimental system for HRPITS measurements at temperatures 20–320 K was based on a Leybold refrigerator cooled optical cryostat and a Keithley 428 fast picoammeter. The photocurrent pulses were generated by a light emitting diode with the spectral characteristic maximum at the wavelength of 650 nm (photon energy 1.96 eV). A typical flux of excitation light was equal to 4.2×10^{15} cm^{-2} s^{-1}. The width of illumination pulses varied from 20 to 30 ms and the period between pulses ranged from 60 to 120 ms. The voltage between two coplanar electrodes was 30 V. Photocurrent transients were digitized with a 12-bit resolution and sampling frequency of 1 MHz. The photocurrent decays were normalized with respect to the photocurrent amplitude at the end of the light pulse. The HRPITS spectra were calculated using the correlation procedure with the implementation of a two-point weighting function $w(t, t_1, t_2) = \delta(t - t_1) - \delta(t - t_2)$. Using various values of t_1 and t_2 (from 1 μs to around 100 ms) and keeping constant values of the ratio t_2/t_1 (e.g. 3), the spectra were determined for a

wide range of emission rate windows from $\sim 4\times10^2$ to $\sim 5\times10^5$ s^{-1}. The broad peaks occurring in the spectra for several emission rate windows were deconvoluted into several separate peaks by means of fitting with Gaussian functions. The physical meaning of each Gaussian peak was verified on the grounds of the shift of this peak with the temperature T for different emission rate windows. This shift should follow the Arrhenius law characteristic of defect centres: $e(T) = AT^2 \exp(-E_a/k_B T)$, where e is the thermal emission rate of electrons or holes, E_a is the trap activation energy, k_B is Boltzmann's constant and A is the pre-exponential factor dependent on the material constant and the apparent capture cross-section for charge carriers.

For each trap detected, we drew the Arrhenius plot of $\log(T^2/e)$ versus $1/T$, the slope of which gave us the trap activation energy E_a and the intercept with the ordinate axis at $1/T = 0$ was equal to the pre-exponential factor A. The traps were tentatively identified by comparing their parameters with the electronic properties of the known defects previously determined in InP by positron annihilation, optical absorption, deep level transient spectroscopy (DLTS) and photoluminescence as well as by TSC and PITS measurements.

Apart from the HRPITS spectra, we analysed the temperature dependence of the photocurrent amplitude at the end of the light pulse. As a result, for each sample a mobility–lifetime product for electrons as a function of temperature was established.

3. Results and discussion

Figure 1 shows the HRPITS spectra of sample 218it characterized by the lowest value of the Hall mobility. Since in the material both shallow and midgap traps predominate, figures 1(a) and (b) illustrate the spectra at the temperature ranges of 20–150 and 150–320 K, respectively. The spectrum in figure 1(a) is given for an emission rate window of 12 300 s^{-1}, corresponding to the ratio of the sampling times $t_1 = 0.1$ ms$/t_2 = 0.3$ ms. The peaks obtained from fitting the part of the spectrum with Gaussian functions are marked with broken curves. The spectrum in figure 1(b) is for an emission rate window of 559 s^{-1}, corresponding to the ratio of the sampling times $t_1 = 2.2$ ms$/t_2 = 6.6$ ms.

The spectrum shown in figure 1(a) indicates that in sample 218it five shallow defects labelled as T1, T2, T3, T6 and T8 with activation energies 10, 20, 50, 100 and 165 meV, respectively, are present. It should be noted that the peak corresponding to trap T1 (10 meV) is approximately three times higher than those related to the other traps. These traps can be either donors or acceptors, and from the HRPITS measurements we cannot distinguish whether the peak is due to the thermal emission of electrons or holes. Figure 1(b) shows the presence of two predominant midgap traps T17 (590 meV) and T18 (640 meV) as well as the presence of trap T12 (280 meV). The peak corresponding to the latter is around seven times lower compared to the peaks observed for traps T17 and T18.

The HRPITS spectrum of sample 21aym at the emission rate window of 2200 s^{-1}, corresponding to the ratio of the sampling times $t_1 = 0.56$ ms$/t_2 = 1.68$ ms, is illustrated in figure 2. It is easily seen that in this material nine defects centres were detected: T2 (20 meV), T3 (50 meV), T6 (100 meV), T7 (140 eV), T8 (165 meV), T9 (195 meV), T15 (520 meV), T17 (590 meV) and T18 (640 meV). Among them the centres T2 (20 meV) and T8 (165 meV) are predominant.

Figure 3 shows the HRPITS spectrum of sample 24asd with the highest value of Hall mobility. The spectrum is presented for an emission rate window of 2200 s^{-1}. The inset shows the part of the spectrum taken at an emission rate window of 12 300 s^{-1} at the temperature range from 20 to 130 K. In this material 12 traps were detected: T1 (10 meV), T3 (50 meV), T4 (60 meV), T5 (80 meV), T10 (240 meV), T11 (265 meV), T12 (280 meV), T13 (350 meV), T14 (500 meV), T16 (530 meV), T17 (590 meV) and T18 (640 meV). Among these defects, trap T14 (500 meV) is predominant.

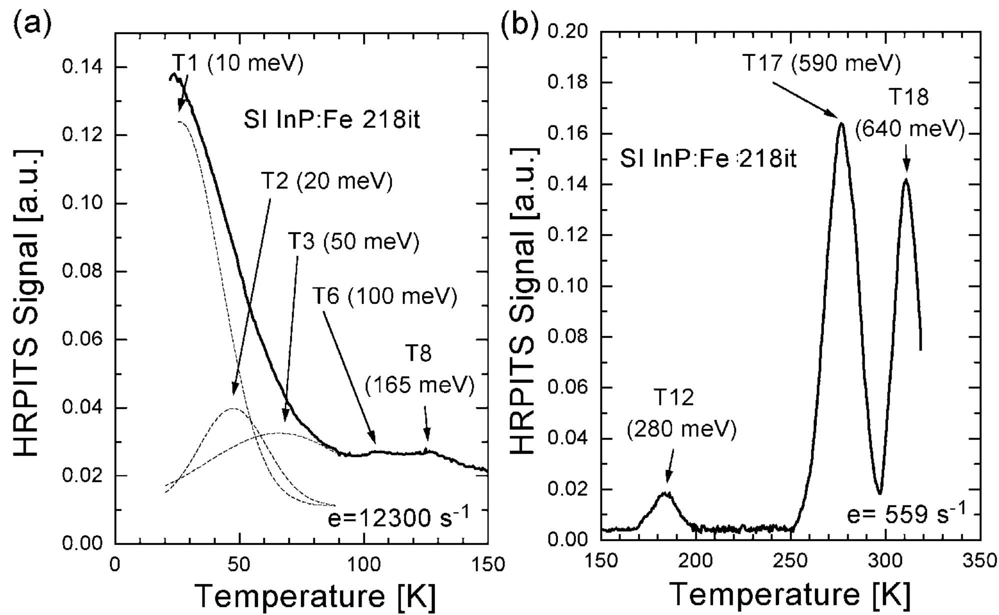

Figure 1. An HRPITS spectrum of SI InP:Fe characterized by Hall mobility at 300 K equal to 1600 cm^2 V^{-1} s^{-1}. (a) temperature range of 20–150 K, emission rate window equal to 12 300 s^{-1}; (b) temperature range of 150–320 K, emission rate window equal to 559 s^{-1}.

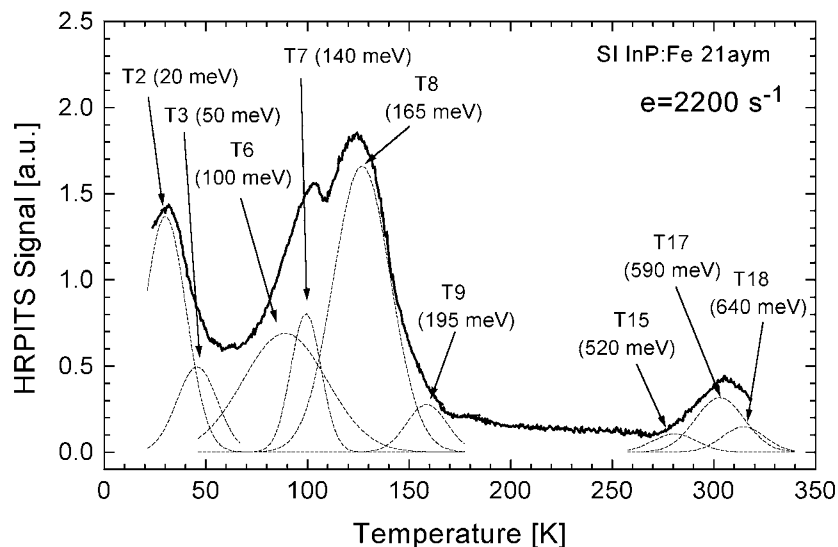

Figure 2. An HRPITS spectrum taken at an emission rate window of 2200 s^{-1} for SI InP:Fe characterized by Hall mobility at 300 K equal to 2392 cm^2 V^{-1} s^{-1}. The peaks obtained from fitting the spectrum with Gaussian functions are marked with broken curves.

The Arrhenius plots for all the traps detected in the samples characterized in table 1 are shown in figures 4(a) and (b). The former illustrates the plots for the traps observed at the temperature range of 20–120 K and the latter presents the plots for the traps detected at the temperature range of 120–320 K. These plots illustrate the dependence of the reciprocal of the

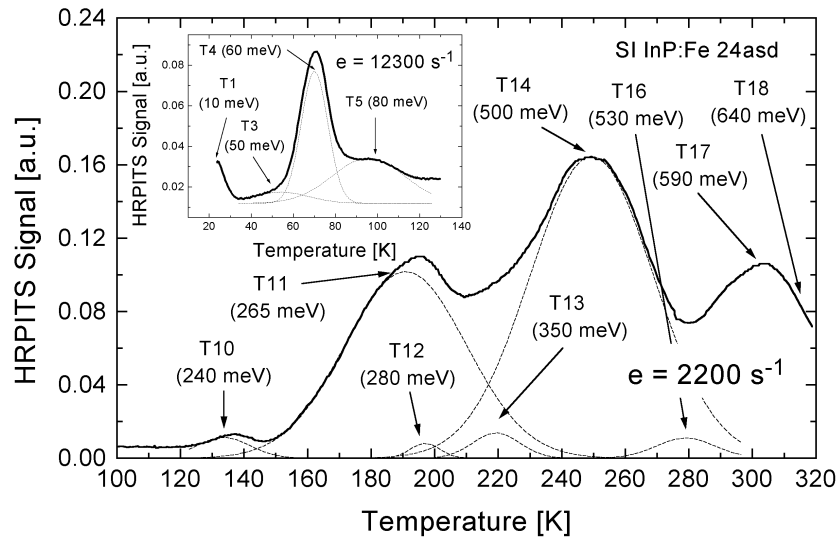

Figure 3. An HRPITS spectrum taken at an emission rate window of 2200 s^{-1} for SI InP:Fe characterized by Hall mobility at 300 K equal to 2638 $cm^2 V^{-1} s^{-1}$. The inset shows the part of the spectrum for the emission rate window of 12 300 s^{-1} determined at the temperature range from 20 to 130 K. The peaks obtained from fitting the spectrum with Gaussian functions are marked with broken curves.

emission rate as a function of the temperature reciprocal, and represent the signatures of the defect centres. The properties of the detected traps determined on the grounds of the Arrhenius plots are summarized in table 2.

The results shown in table 2 indicate that the defect structure of SI InP:Fe is very complex and the material properties are affected by a number of various point defects. Trap T1 (10 meV) is likely to be attributed to shallow donor impurities such as sulfur in the phosphorus sublattice or silicon in the indium sublattice [6, 7]. The ionization energy of these donors is around 6 meV [7]. Trap T2 (20 meV) can be assigned to shallow acceptor impurities such as silicon in the phosphorus sublattice or zinc in the indium sublattice [6, 7]. The ionization energy of these acceptors is around 30 meV [7]. Moreover, the results of glow discharge mass spectroscopy (GDMS) indicate that InP crystals are contaminated mainly with sulfur, silicon and zinc and the amount of sulfur is much higher than that of silicon and zinc [15]. On the other hand, it has been suggested that iron in InP is compensated by a shallow donor related to the 2316 cm^{-1} local vibration mode (LVM) assigned to the fully hydrogenated indium vacancy $V_{In}H_4$ [16]. Trap T3 (50 meV) is presumably another shallow donor formed, however, by a native defect or a native defect–impurity complex [6, 7]. Traps T4 (60 meV) and T5 (80 meV) we assumed as unknown, for we have not managed to find any reference on the properties to defects corresponding to these traps. The activation energies of traps T6 (100 meV) and T7 (140 meV) match very well the ionization levels $E_v + 0.1$ eV and $E_v + 0.13$ eV of indium vacancies $V_{In}^{0/+}$ and $V_{In}^{-/0}$, respectively [8]. Traps T8–T16, with activation energies ranging from 165 to 530 meV, are likely to be attributed to native defects or complexes involving a native defect and an impurity. The two midgap traps T17 (590 meV) and T18 (640 meV) are related to iron Fe^{2+} [14]. The former is likely to be attributed to the complex composed of Fe^{2+} and a native defect [12, 13], while the latter corresponds to the transition $Fe^{2+} \rightarrow Fe^{3+} + e^-$ [14].

The spectra presented in figures 1–3 illustrate the differences in the defect structure of SI InP:Fe crystals with various Hall mobility. In the crystal with the lowest Hall mobility

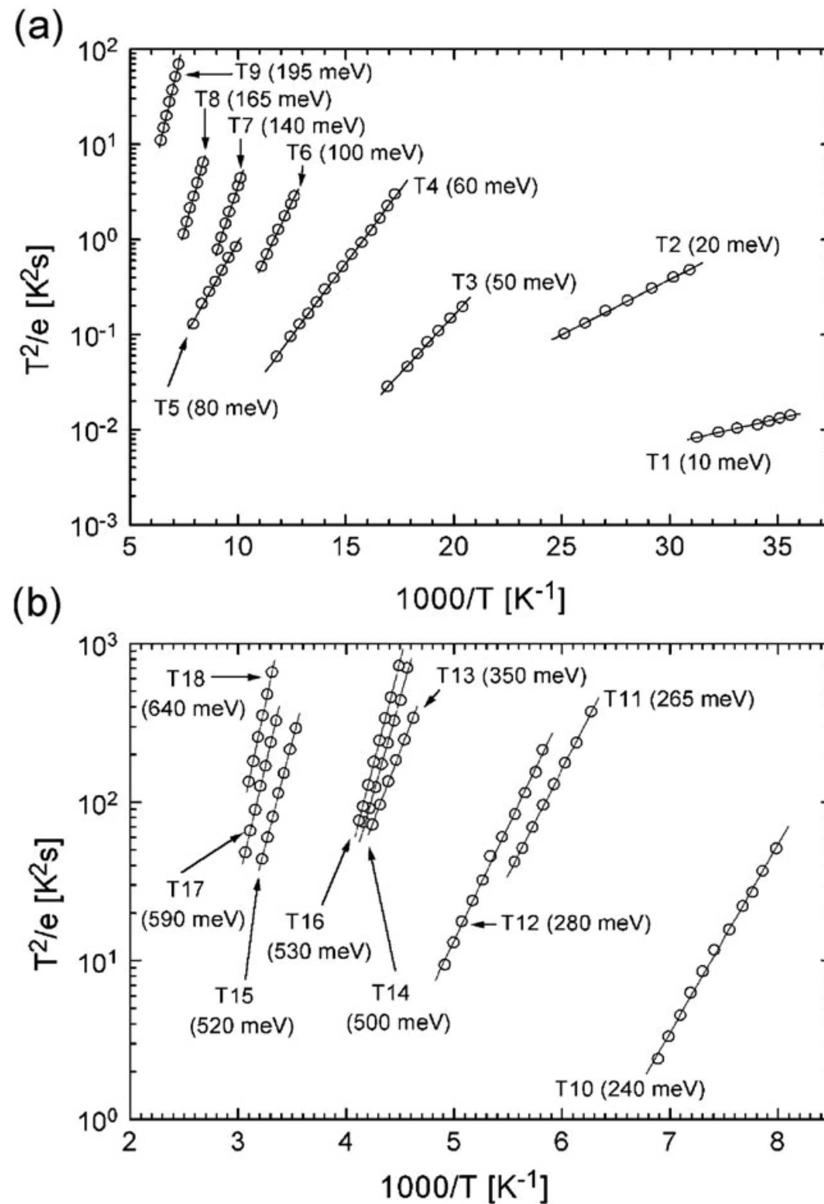

Figure 4. Arrhenius plots for grow-in point defects detected in SI InP:Fe. (a) temperature range of 20–120 K; (b) temperature range of 120–320 K.

(1600 cm^2 V^{-1} s^{-1}), shallow donor impurities and iron-related defects are mainly observed. It should be emphasized that the higher concentration of shallow donors results in a higher concentration of Fe^{2+} and a lower concentration of Fe^{3+}.

In the crystal with Hall mobility 2392 cm^2 V^{-1} s^{-1}, the shallow donor impurities are not observed, and dominant defects include shallow acceptors and native defects. The small peaks related to Fe^{2+} indicate that the vast majority of iron atoms are in the Fe^{3+} charge state. So, the mobility in this crystal is limited mainly by the high total concentration of iron (4×10^{16} cm^{-3})

Table 2. Summary of HRPITS results on parameters of traps detected in SI InP:Fe grown by the LEC method. (Comments: e and h denote electron and hole trap, respectively)

Trap label	Activation energy E_a (meV)	Pre-exponential factor A (s^{-1} K^{-2})	Tentative identification	Material in which the trap occurs
T1	10	5.0×10^3	Shallow donors: S, Si [6, 7]	218it and 24asd
T2	20	5.0×10^3	Shallow acceptors: Si, Zn [6, 7]	218it and 21aym
T3	50	1.0×10^5	Shallow donor: native defect or native defect–impurity complex [6, 7]	218it, 24asd and 21aym
T4	60	7.0×10^4	Unknown	24asd
T5	80	1.0×10^4	Unknown	24asd
T6	100	1.0×10^5	$V_{In}^{0/+}$ [8]	218it and 21aym
T7	140	3.0×10^6	$V_{In}^{-/0}$ [8]	21aym
T8	165	1.5×10^6	Native defect observed after electron irradiation (h) [9]; D0 (e) in [10]	218it and 21aym
T9	195	2.0×10^5	Related to V_P (e) [11]	21aym
T10	240	6.5×10^7	$P_{In}^{+/2+}$ [12]	24asd
T11	265	6.5×10^5	Related to Zn [9]	24asd
T12	280	4.0×10^5	E6 in [13]	218it and 24asd
T13	350	4.0×10^6	Related to P_{In} (e) [11]	24asd
T14	500	3.0×10^8	Fe–donor complex (e) [12]	24asd
T15	520	7.0×10^6	P_{In}–Zn complex (h) [9]	21aym
T16	530	1.0×10^9	Induced by excess of P [9]	24asd
T17	590	3.0×10^8	Complex involving Fe^{2+}; B2 (e) [12], E1 [13]	218it, 24asd and 21aym
T18	640	4.0×10^8	$Fe^{2+/3+}$(e) [14]	218it, 24asd and 21aym

which is the sum of [Fe^{2+}] + [Fe^{3+}]. The crystal with Hall mobility 2638 cm^2 V^{-1} s^{-1} contains small shallow donor concentration as well as small iron concentration (9×10^{15} cm^{-3}). The dominant defects in this material are related to its stoichiometry and are formed by complexes involving the phosphorus antisite (P_{In}).

Figure 5 gives the comparison of the electron mobility–lifetime product ($\mu\tau$) as a function of temperature for all the samples characterized in table 1. It is easily seen that for each sample we have a different value of the $\mu\tau$ product at room temperature (300 K) and different behaviour with decreasing temperature from 300 to 30 K. The values of the electron lifetime at 300 K calculated for samples 218it, 21aym and 24asd are 2.2×10^{-9}, 2.4×10^{-10} and 3.2×10^{-9} s, respectively. So, the lifetime at 300 K is determined mainly by the iron concentration. With decreasing temperature, the lifetime begins to decrease due to decreasing the carrier emission rate from the iron-related recombination centres. Next, while the temperature decreases the majority of iron-related centres become occupied. Thus, at a temperature below 200 K the lifetime starts to be determined by band-to-acceptor (BA), band-to-band (BB), donor–acceptor (DA) and donor-to-band (DB) transitions. The probability of these transitions decreases with decreasing temperature and the lifetime increases [6, 17]. To some extent, the temperature dependence of the $\mu\tau$ product is also affected by the changes in the electron mobility. In InP crystals with net donor concentration $\sim 1 \times 10^{16}$ cm^{-3} the Hall mobility may rise up to 4 times on decreasing the temperature from 300 to 70 K [7]. So, the variations of the $\mu\tau$ product at the temperature range from 100 to below 50 K reflect the changes of the mobility.

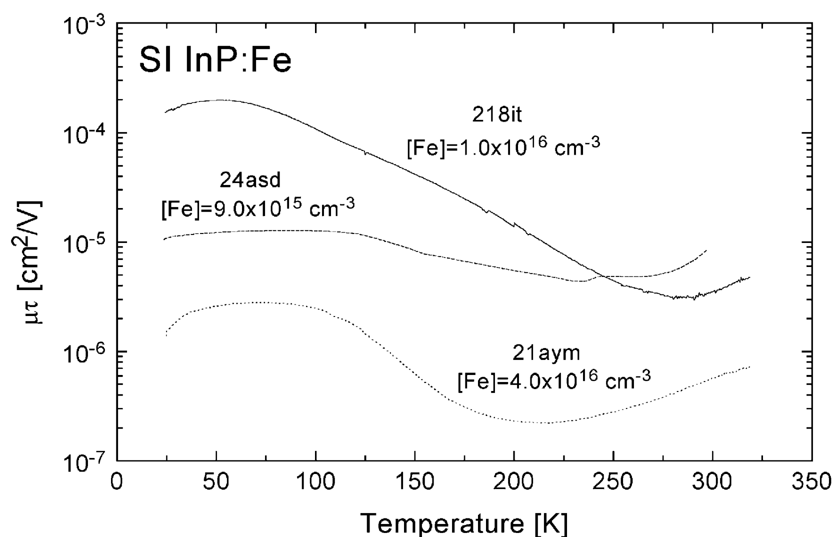

Figure 5. Mobility–lifetime product for electrons as a function of temperature for samples of SI InP:Fe with various iron concentration.

4. Conclusions

HRPITS has been employed to compare the defect structure of SI InP:Fe crystals with various Hall mobility. Eighteen defect centres with activation energies ranging from 10 to 640 meV were detected. These centres are tentatively identified as shallow donor and acceptor impurities, shallow native defects, complexes involving native defects, and iron-related centres. In the crystal with Hall mobility 1600 $cm^2\ V^{-1}\ s^{-1}$, the dominant defects are the shallow donor impurities and iron Fe^{2+} centres. The defect structure of the material with Hall mobility 2392 $cm^2\ V^{-1}\ s^{-1}$ is constituted by shallow acceptor impurities, complexes involving native defects, and iron centres in the Fe^{3+} charge state. In the case of the crystal with Hall mobility 2638 $cm^2\ V^{-1}\ s^{-1}$ there is a balance between the shallow donor impurities and the iron centres in Fe^{2+} charge states, and the dominant defects are related to complexes involving the phosphorus antisite (P_{In}).

Acknowledgment

This research has been supported by the Polish Committee for Scientific Research under Grant No 4 T11B 068 24.

References

[1] Kubota E, Ando K and Yamada S 2000 *J. Appl. Phys.* **87** 2885–9
[2] Chen W M, Dreszer P, Prasad A, Kurpiewski A, Walukiewicz W, Weber E R, Sorman E, Monemar B, Liang B W and Tu C W 1994 *J. Appl. Phys.* **76** 600–2
[3] Kaminski P, Pawlowski M, Cwirko R, Palczewska M and Kozlowski R 1996 *Mater. Sci. Eng.* B **42** 213–6
[4] Hurtes Ch, Boulou M, Mitonneau A and Bois D 1978 *Appl. Phys. Lett.* **32** 821–3
[5] Fairman R D, Morin F J and Oliver J R 1979 *Ins. Phys. Conf. Ser.* **45** 134–43 chapter 2
[6] Mayer K M, Makita Y, Yamada A, Shibata H, Beye A C and Shimada J 1992 *J. Appl. Phys.* **72** 1080–5

[7] Shmidt N M 1996 *Handbook Series on Semiconductor Parameters* vol 1, ed M Levinshtein, S Rumyantsev and M Shur (London: World Scientific) pp 169–90
[8] Polity A and Engelbrecht T 1997 *Phys. Rev.* B **55** 10480–6
[9] Katz A (ed) 1992 *Indium Phosphide and Related Materials: Processing, Technology, and Devices* (Boston, MA: Artech House Publishers) pp 75–102
[10] Marrakchi G, Cherkaoui K, Karoui A, Hirt G and Muller G 1996 *J. Appl. Phys.* **79** 6947–50
[11] Fang Z Q, Look D C, Uchida M, Kainosho K and Oda O 1998 *J. Electron. Mater.* **27** L68–71
[12] Fornari R, Brinciotti A, Gombia E, Mosca R and Sentiri A 1994 *Mater. Sci. Eng.* B **28** 95–100
[13] Nicholas D J, Allsopp D, Hamilton B, Peaker A R and Bass S J 1984 *J. Cryst. Growth* **68** 326–33
[14] Kaminski P and Thomas H 1990 *Acta Phys. Pol.* A **77** 87–90
[15] Zdansky K, Pekarek L and Kacerovsky P 2000 *Proc. 2000 IEEE NSS Lyon* (Piscataway, NJ: IEEE) pp 4132–6
[16] Ewels C P, Oberg S, Jones R, Pajot B and Briddon P R 1996 *Semicond. Sci. Technol.* **11** 502–7
[17] Liu A and Rosenwaks Y 1999 *J. Appl. Phys.* **86** 430–7